



Nonvolcanic seafloor spreading and corner-flow rotation accommodated by extensional faulting at 15°N on the Mid-Atlantic Ridge: A structural synthesis of ODP Leg 209

Timothy Schroeder

Environmental Earth Science Department, Eastern Connecticut State University, 83 Windham Street, Willimantic, Connecticut 06226, USA (schroedert@easternct.edu)

Michael J. Cheadle

Department of Geology and Geophysics, University of Wyoming, Laramie, Wyoming 82701, USA

Henry J. B. Dick

Department of Geology and Geophysics, Woods Hole Oceanographic Institution, McLean Laboratory, Room 214, Woods Hole, Massachusetts 02543, USA

Ulrich Faul

Department of Earth Sciences, Boston University, 675 Commonwealth Avenue, Boston, Massachusetts 02215, USA

John F. Casey

Department of Geosciences, University of Houston, Houston, Texas 77204, USA

Peter B. Kelemen

Lamont-Doherty Earth Observatory, Columbia University, 58 Geochemistry Building, Palisades, New York 10964, USA

[1] Drilling during ODP Leg 209, dredging, and submersible dives have delineated an anomalous stretch of the Mid-Atlantic Ridge north and south of the 15°20'N Fracture Zone. The seafloor here consists dominantly of mantle peridotite with gabbroic intrusions that in places is covered by a thin, discontinuous extrusive volcanic layer. Thick lithosphere (10–20 km) in this region inhibits magma from reaching shallow levels beneath the ridge axis, thereby causing plate accretion to be accommodated by extensional faulting rather than magmatism. The bathymetry and complex fault relations in the drill-core suggest that mantle denudation and spreading are accommodated by a combination of high-displacement, rolling-hinge normal faults and secondary lower-displacement normal faults. These extensional faults must also accommodate corner flow rotation (up to 90°) of the upwelling mantle within the shallow lithosphere, consistent with remnant magnetic inclinations in denuded peridotite and gabbro from Leg 209 core that indicate up to 90° of sub-Curie-temperature rotation.

Components: 8457 words, 9 figures.

Keywords: seafloor spreading; ocean drilling program; nonvolcanic mid-ocean ridges; extensional faulting.

Index Terms: 3035 Marine Geology and Geophysics: Midocean ridge processes; 3040 Marine Geology and Geophysics: Plate tectonics (8150, 8155, 8157, 8158); 3036 Marine Geology and Geophysics: Ocean drilling.

Received 22 December 2006; **Revised** 9 March 2007; **Accepted** 6 April 2007; **Published** 28 June 2007.

Schroeder, T., M. J. Cheadle, H. J. B. Dick, U. Faul, J. F. Casey, and P. B. Kelemen (2007), Nonvolcanic seafloor spreading and corner-flow rotation accommodated by extensional faulting at 15°N on the Mid-Atlantic Ridge: A structural synthesis of ODP Leg 209, *Geochem. Geophys. Geosyst.*, 8, Q06015, doi:10.1029/2006GC001567.

1. Introduction

[2] Plate accretion at mid-ocean ridges can be described by two general end-member processes: normal magmatic accretion (“volcanic spreading”), or tectonic denudation of mantle rocks (“nonvolcanic spreading”). During volcanic spreading, a continuous mafic crust is constructed by volcanism and shallow magma intrusion (Figure 1a) [e.g., *Sinton and Detrick*, 1992]. During “nonvolcanic” spreading, extensional faulting denudes an upper lithosphere composed dominantly of ultramafic mantle rocks containing gabbro plutons that were intruded and solidified at deeper levels (Figure 1b) [*Cannat et al.*, 1992; *Cannat*, 1993; *Smith and Cann*, 1993; *Thatcher and Hill*, 1995; *Karson*, 1999; *Buck et al.*, 2005]. Volcanic spreading is the norm at fast spreading and most sections of intermediate- and slow-spreading ridges [*Sinton and Detrick*, 1992]. Nonvolcanic spreading occurs in regions of thick, cold lithosphere on slow spreading ridges [*Dick et al.*, 1981; *Cannat*, 1993; *Cannat et al.*, 1997; *Tucholke and Lin*, 1994; *Cann et al.*, 1997; *Lagabrielle et al.*, 1998; *Tucholke et al.*, 1998; *Ranero and Reston*, 1999; *Smith et al.*, 2006], and may be widespread at ultra-slow spreading ridges [*Dick et al.*, 2003; *Cannat et al.*, 2006].

[3] Here, we summarize structural results from ODP Leg 209, which drilled a nonvolcanic section of the Mid-Atlantic Ridge (MAR) near the 15°20′ Fracture Zone (FZ), and suggest how these results place constraints on fault-accommodated nonvolcanic spreading. The 15°20′ FZ region has been shown by geophysical studies to contain very thin or no magmatic crust [*Rona et al.*, 1987; *Escartín and Cannat*, 1999; *Matsumoto et al.*, 1998; *Fujiwara et al.*, 2003], and dredging and submersible sampling indicates that gabbro and mantle peridotite is exposed on over 50% of the area (Figure 2) [*Cannat et al.*, 1995, 1997; *Casey et al.*, 1998; *Kelemen et al.*, 1998; *Lagabrielle et al.*, 1998; *Fujiwara et al.*, 2003]. In the absence of diapirism, it is not possible for gabbro or mantle peridotite to undergo ductile flow to the surface; and so in a mid-ocean ridge environment they can only be exposed in the foot-

wall of a normal fault. Consequently much of the seafloor in this region must be composed of fault surfaces; a conclusion supported by the common presence of fault rocks on these surfaces [*Kelemen et al.*, 1998; *Fujiwara et al.*, 2003; *Escartín et al.*, 2003]. Submersible outcrop observations suggest that most exposed basalt in the area is a thin carapace that erupted onto a fault surface, beneath which lies gabbro or peridotite [*Cannat et al.*, 1997].

[4] Anomalous magnetic remanence vector inclinations (i.e., lower than the expected geocentric axial dipole inclination of +28°) measured in Leg 209 core indicate that below Curie temperature tectonic rotation occurred in this region, presumably associated with extensional faulting [*Garces and Gee*, 2007]. If it is assumed that the inclinations were changed by rotation about horizontal, or near horizontal, axes parallel to the strike of the prominent faults visible in bathymetry, and that the rotation sense is “top away from the ridge axis,” then 50° to 80° of postmagnetization rotation is required at ODP Sites 1268, 1270, 1274 and 1275 [*Kelemen et al.*, 2004; *Garces and Gee*, 2007]. Significant tectonic rotations are also possible for Sites 1271 and 1272. Serpentinized peridotites from these sites yield average magnetic vector inclinations similar to the present-day geocentric axial dipole inclination. Although this result is consistent with no rotation, it is equally consistent with rotations of 40–50°, because rotation about an axis which is not parallel to direction of the magnetic field will yield an inclination similar to the prerotation inclination [see *Garces and Gee*, 2007, Figure 3]. The important result from the magnetic measurements is that although the orientation of the rotation axis for each individual drill site is poorly constrained, the observation that many of the cores have an anomalous magnetic inclination is strong evidence that tectonic rotation is widespread in the region drilled during ODP Leg 209 [*Garces and Gee*, 2007].

[5] The sub-Curie-temperature tectonic rotation indicated by the core is consistent with mantle corner flow occurring in the shallow lithosphere during nonvolcanic spreading. Plate divergence at mid-ocean ridges causes the upwelling mantle to

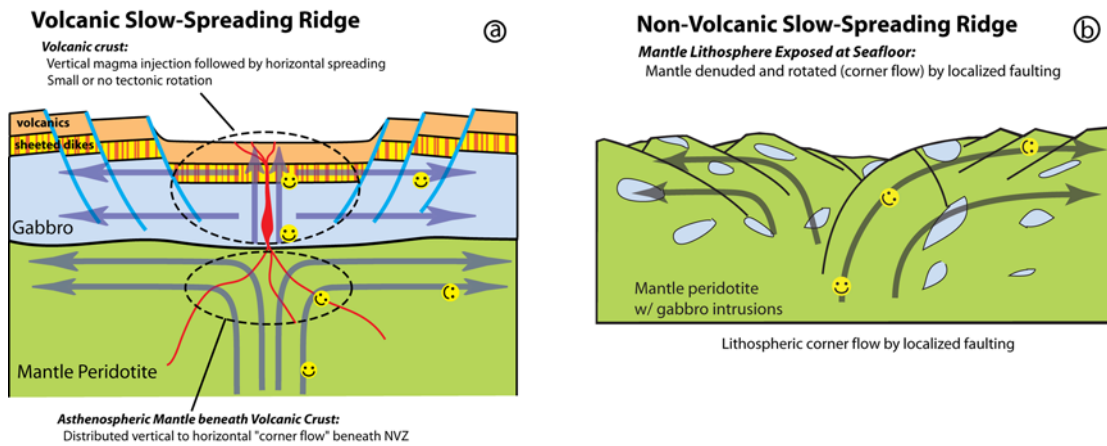


Figure 1. Cartoons depicting mantle corner flow at (a) a “normal” volcanic ridge and (b) a “nonvolcanic” ridge. At the volcanic ridge, corner flow occurs via distributed deformation beneath the magmatic crust. At the nonvolcanic ridge, corner flow occurs via localized faulting in the shallow lithosphere.

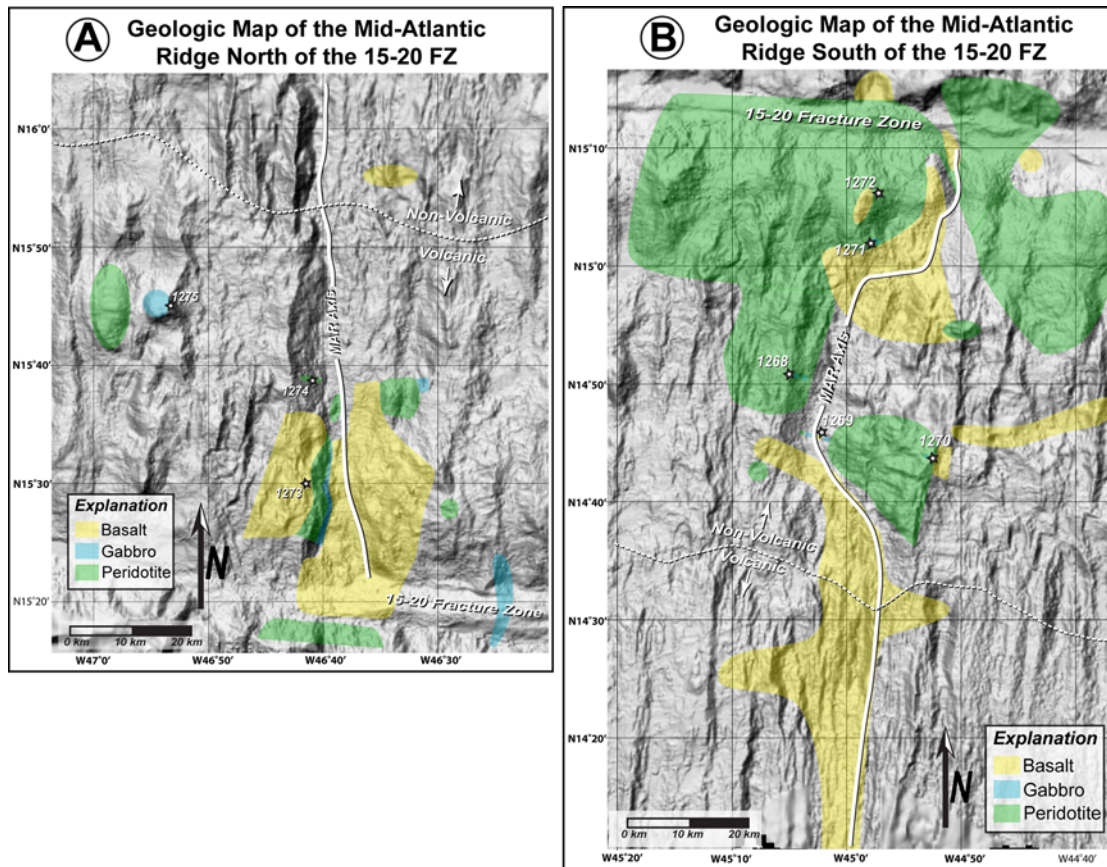


Figure 2. Geologic maps of regions (a) north of the 15°20' FZ and (b) south of the 15°20' FZ. Lithology information was compiled from submersible dive tracks performed on the 1992 Faranaut Cruise [Cannat et al., 1997], submersible dives and dredge hauls performed on the MODE98 Cruise [Kelemen et al. 1998], and dredge hauls from several earlier cruises [Rona et al., 1987; Skolotnev et al., 1989].

undergo $\sim 90^\circ$ of corner flow rotation beneath the ridge axis. At volcanic ridges, corner flow occurs by distributed deformation within the upper asthenosphere (Figure 1a). Crust formed by volcanic spreading does not undergo corner flow rotation, as it accretes by vertical magma intrusion followed by lateral spreading. Logically, where no magmatic crust is present and the lithosphere is thick, corner flow would occur by localized deformation within the shallow lithosphere (Figure 1b).

2. Bathymetry of the $15^\circ 20'$ Fracture Zone Region

[6] Volcanic and nonvolcanic seafloor can be recognized in the $15^\circ 20'$ FZ region bathymetry (Figure 2). *Cannat et al.* [1997] and *Fujiwara et al.* [2003] used bathymetry to define volcanic seafloor (>60 km south and >50 km north of the transform) and nonvolcanic areas north and south of the transform. A statistical slope-aspect distribution analysis of $15^\circ 20'$ FZ bathymetry shows that the orientation of steep slopes (interpreted to be normal fault sets) is different in seafloor produced by volcanic and nonvolcanic spreading. This analysis was performed by isolating bathymetric data in areas of volcanic and nonvolcanic seafloor on the east and west sides of the MAR, and calculating eight-neighbor directional slopes at each bathymetry grid point with the computer program MicroDEM [*Guth*, 2003]. Binned directional slope values plotted on rose diagrams are shown with bathymetry in Figures 4 and 5. No slopes steeper than 45° are recorded in any location. This may be due to the effect of slope smoothing by the Seabeam data acquisition method, and/or mass wasting leading to a shallowing of steep slopes (Figure 3).

[7] The bathymetry in the constructional volcanic terrain shows strongly ridge-parallel lineated terrain dimpled by small cones and linear ridges cut by numerous small offset normal faults. Major terrain-forming features consist of closely spaced (1–3 km) relatively steep ($\sim 25^\circ$) inward facing scarps with intervening gentler outward facing slopes (Figure 2). The former likely consist of sets of sediment draped mass wasted normal fault scarps, representing 100–500 m total vertical throw, and the latter of back-tilted constructional volcanic terrain (Figure 3). Slope distributions in the volcanic-spreading areas are asymmetrical; shallow slopes ($<20^\circ$) dip preferentially away from the ridge axis, and steeper slopes ($>20^\circ$) dip dominantly toward the ridge axis. Small-

displacement normal fault sets active during volcanic spreading dip predominantly toward the ridge axis and produce only minor footwall rotation (5° – 10°) of volcanic surfaces away from the ridge creating the asymmetric slope aspect distribution patterns.

[8] The nonvolcanic bathymetry lacks the numerous small cones, lineated ridges, and ubiquitous small offset normal faults, and is characterized by more widely spaced (2–10 km) gentler dipping ($\sim 15^\circ$) relatively smooth slopes. These smooth slopes appear to represent rotated fault scarps with 500–1,000 m of vertical throw, and total slip between 1000 m and 15 km (average slip = 2,050 m). In this nonvolcanic “smooth” terrain, the shallow slopes have a nearly symmetrical distribution, dipping both toward and away from the ridge axis to a similar degree. However, the steeper slopes tend to dip away from the ridge axis (Figures 4 and 5). Both these observations, together with the overall form of the bathymetry, are consistent with nonvolcanic seafloor generated by slip on large-displacement faults that undergo greater slip and more rotation than faults cutting the volcanic terrain. Steeper slopes that dip away from the ridge axis may correspond to later, high-angle faults that cut the low angle fault surfaces [e.g., *Tucholke et al.*, 2005], or may be fault surfaces that originally dipped toward the ridge but have been significantly rotated by later faulting. The nonvolcanic bathymetry in this region is similar to the “smooth” bathymetry documented at the Southwest Indian Ridge by *Cannat et al.* [2006]. Both exhibit large 10–20 km wide low-relief surfaces, both have steeper outward facing scarps, and both expose mantle peridotite and/or gabbro at the seafloor. While total relief in the smooth nonvolcanic regions is actually greater than in volcanic terrains, the texture and roughness of the seafloor is very different, with long gentle slopes and far broader fault spacing.

[9] The nonvolcanic bathymetry near the $15^\circ 20'$ FZ can be visually subdivided into two further categories: widely spaced ridges (or “smooth bathymetry”) and corrugated domes. The bulk (97%) of the nonvolcanic area comprises the “smooth” widely spaced ridges. Corrugated domes (outlined in Figures 4 and 5) extend 10 to 20 km parallel to the ridge axis and ~ 10 km wide, with 5 – 10° slopes and linear corrugations parallel to the spreading direction. These domes have been previously recognized as oceanic core complexes [*MacLeod et al.*, 2002; *Escarotín et al.*, 2003; *Fujiwara et al.*, 2003], but represent $<3\%$ of the

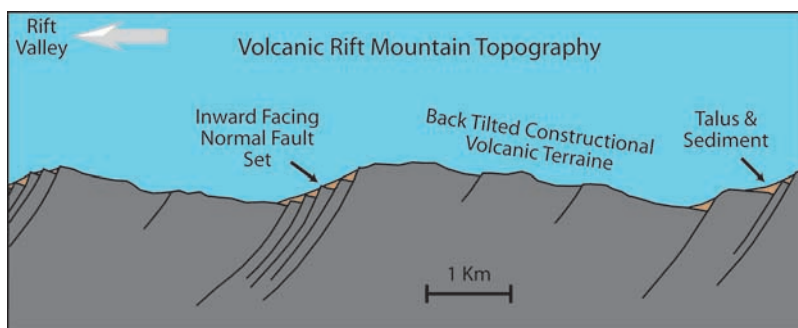


Figure 3. Schematic cross section showing high-angle normal faults sets in volcanic terrain that after mass wasting approximate a lower-angle slope.

nonvolcanic bathymetry in this region (from 14°30'N to 16°N). A similar percentage (4%) of the seafloor comprises corrugated domes on the nonvolcanic section of the Southwest Indian Ridge

surveyed by *Cannat et al.* [2006]. We suggest that the corrugated domes between 14°30' and 16°N on the MAR are a subset of the smooth terrain rather

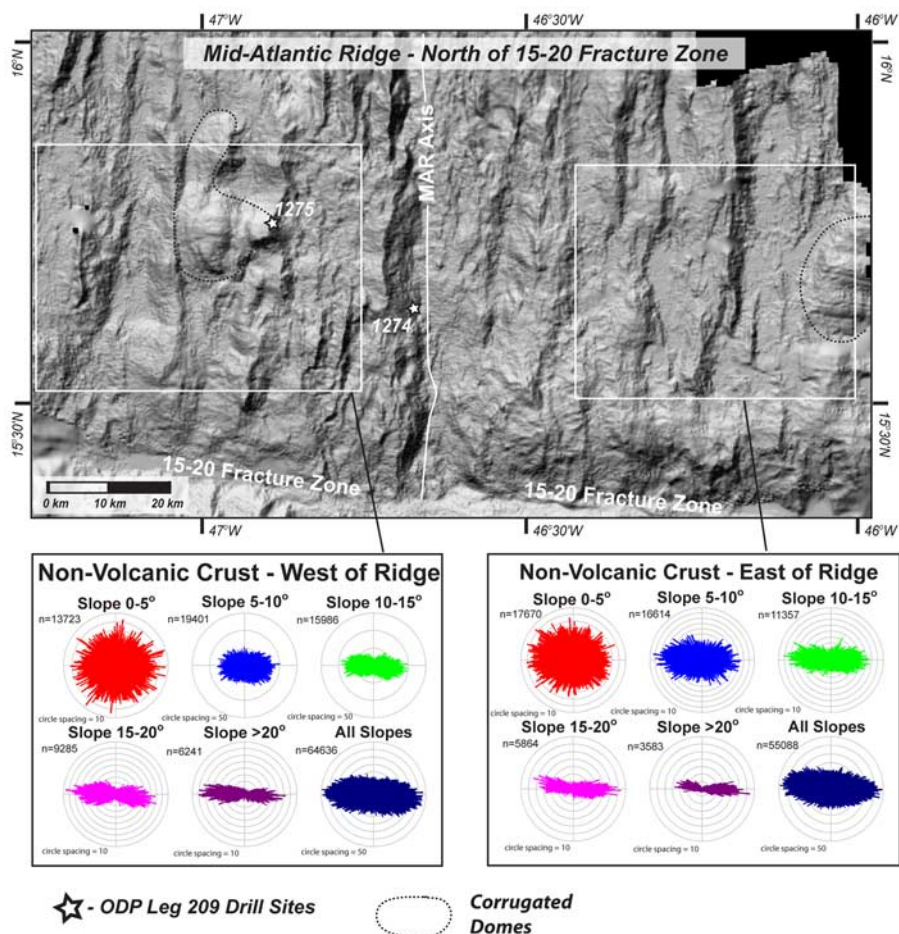


Figure 4. Bathymetric map of the study region north of the 15°20' Fracture Zone with binned slope aspect distribution rose (radial data density) diagrams. Directional slopes were calculated across isolated regions of the bathymetry data set (all within volcanic or nonvolcanic areas on one side of the ridge axis) with an 8-neighbor algorithm. Areas outlined by boxes represent the regions of bathymetry isolated for the slope-aspect distribution analysis. Corrugated, oceanic core complex domes are outlined by dashed lines.

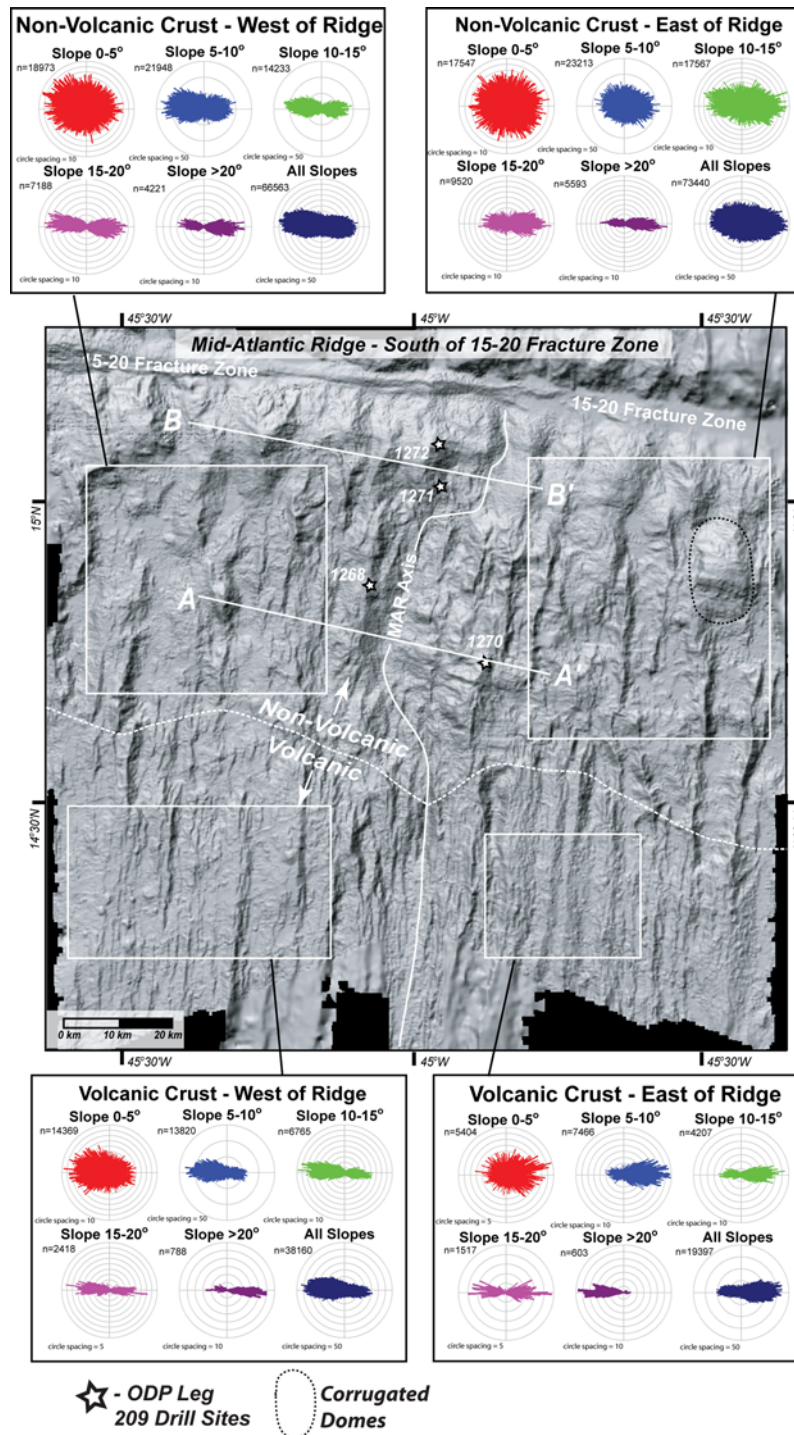


Figure 5. Bathymetric map of the study region south of the $15^{\circ}20'$ Fracture Zone with binned slope aspect distribution rose (radial data density) diagrams. Directional slopes were calculated across isolated regions of the bathymetry data set (all within volcanic or nonvolcanic areas on one side of the ridge axis) with an 8-neighbor algorithm. Areas outlined by boxes represent the regions of bathymetry isolated for the slope-aspect distribution analysis. Corrugated, oceanic core complex domes are outlined by dashed lines. Rose diagrams show different distribution in the dip directions (toward or away from the ridge axis) of varying steepness seafloor slopes in volcanic versus nonvolcanic regions. The border between areas of volcanic and nonvolcanic spreading south of the transform is shown with a dashed white line. Lines of section A-A' and B-B' from Figure 9 are shown on the bathymetry map.

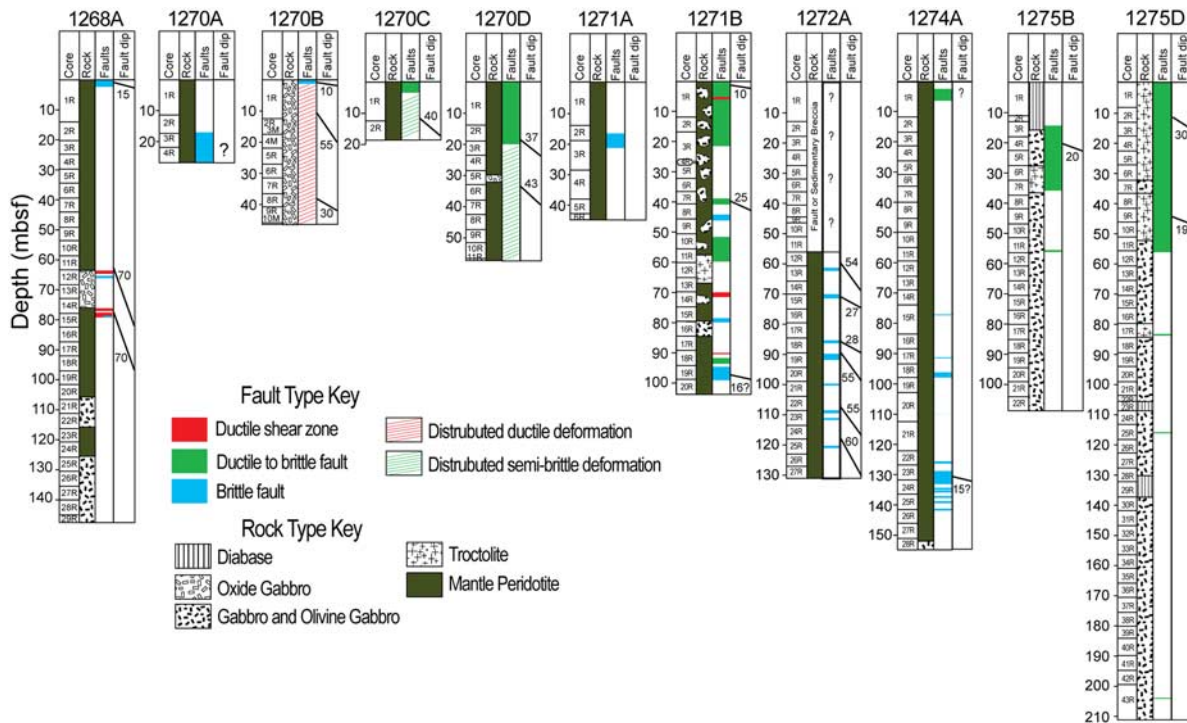


Figure 6. Borehole fault logs from ODP Leg 209. The left column for each hole indicates the dominant rock type in regions of that hole. The middle column for each hole indicates the location and type of faults. The right column for each hole indicates the dip of the fault if it was able to be determined in the core or by borehole logging.

than a separate terrain as *Cannat et al.* [2006] suggest.

3. Faults and Shear Zones in ODP Leg 209 Core

[10] During ODP leg 209, five sites were drilled into the smooth nonvolcanic terrain (1268, 1270, 1271, 1272 and 1274), one into the domal core complex terrain [1275], and two into basalt flows on top of the smooth terrain encountered numerous faults and shear zones, and in several cases bottomed out in a fault zone, providing evidence for the nature of faulting in this terrain. Below are summarized the major faults encountered at each of these sites. The fault distribution in holes and their dips (where known) are shown in Figure 6. The dip of the faults and shear zones were determined by measuring the apparent dips of structures in the cut face of the core and in one other direction (commonly perpendicular to the cut face), then calculating its true dip.

3.1. Site 1268

[11] Hole 1268A was drilled west of the ridge axis on a 15° east-dipping fault scarp with ~ 3 km of displacement (Figure 5) measured in a bathymetric profile perpendicular to the ridge axis. The first core contains a brittle fault consisting of cohesive cataclases. The hole also intersects three (~ 1.5 m wide) ductile, peridotite mylonite shear zones at the upper and lower bounds of a gabbro intrusion that extends from 63 to 78 meters below seafloor (mbsf) (Figures 6 and 7). The foliation of the shear zones dips $\sim 50^\circ$ – 65° . These mylonites were statically serpentinized, and two are cut by <0.5 m wide brittle faults consisting of serpentinite gouge. The fault rocks recovered from the top of the hole most likely represent the 3 km displacement fault visible in seafloor bathymetry. Ductile and brittle faults deeper in the hole may be splays of this major fault, or may be the result of internal block deformation due to flexural footwall rotation. Submersible observations up this slope on Shinkai 6500 dive 427 during the MODE98 Cruise [*Kelemen et al.*, 1998] indicate that the slope is continuous with few scarps or breaks in slope. This suggests that few secondary faults cut the primary, high-displacement fault in this area.

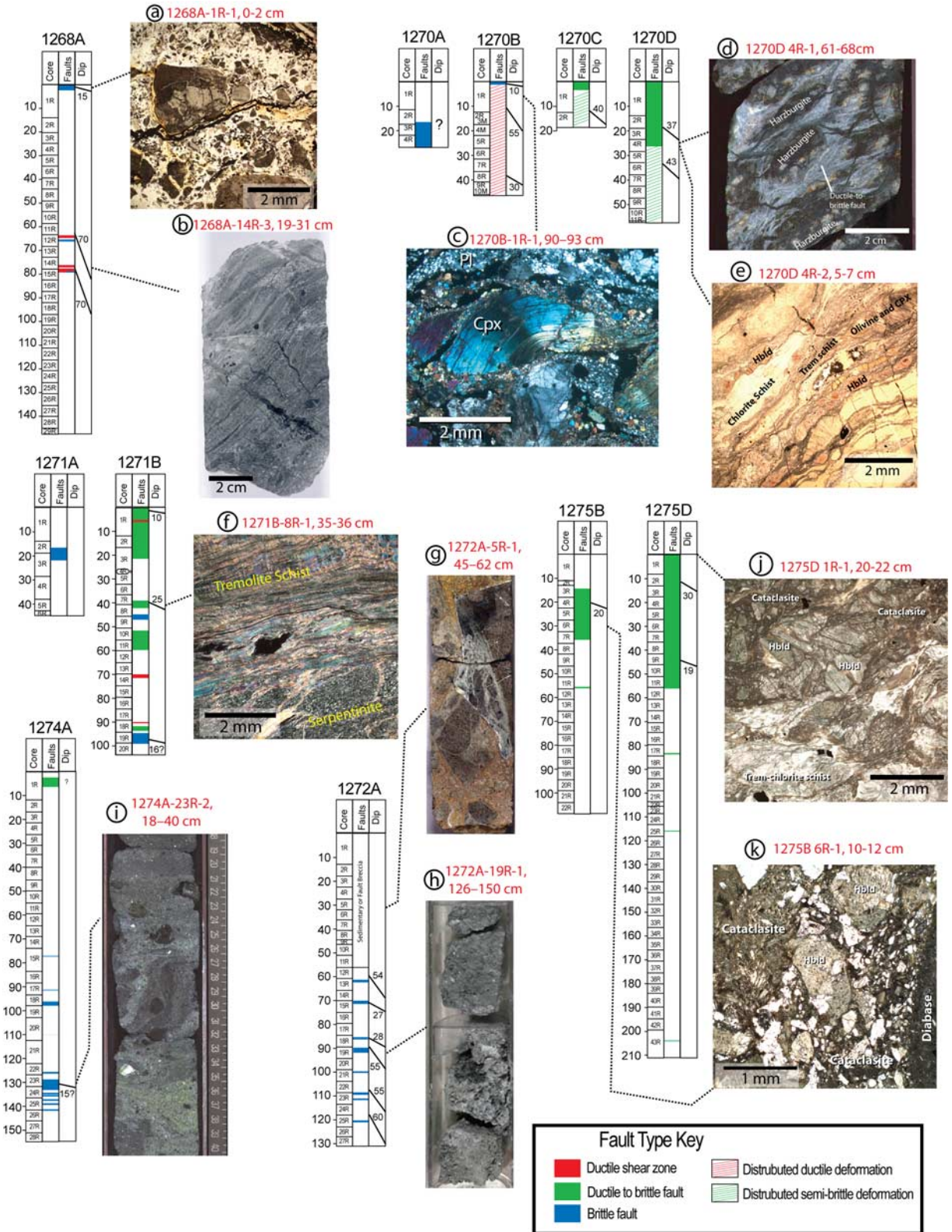


Figure 7

3.2. Site 1270

[12] Four holes at Site 1270 were drilled 12 km east of the MAR axis near the crest of a 2,500 m vertical relief ridge (Figure 5). The average dip of the ridge's western slope (toward the axial valley) is 10° measured in a ridge-perpendicular bathymetric profile. Submersible sampling along this slope by the Shinkai 6500 during dive 425 of the MODE98 cruise recovered several samples of peridotite mylonite (Figure 8), leading investigators to propose that the slope is an exposed detachment fault [Kelemen *et al.*, 1998; Fujiwara *et al.*, 2003]. We concur with this interpretation, but suggest that the ridge is a single large fault surface and not a domal oceanic core complex. Inspection of the bathymetry in Figure 5 shows a relatively smooth constant westward dip from the crest of the eastern rift valley wall to its base, broken by outward facing normal faults. The slope exhibits a series of scarps parallel and oblique (up to 25°) to the axial valley that may be secondary faults cutting the main fault surface. Hole 1270A bottomed out in a brittle fault (cataclasite and gouge) cutting serpentinite at ~ 17 mbsf. Hole 1270B contains several, moderate-intensity ductile shear zones and other areas of distributed, low-intensity ductile deformation that dip between 30° to 50° . The upper portions of Holes 1270C and D

contain numerous high-intensity, ductile-to-brittle faults. Many other thin (1 cm wide) ductile-to-brittle faults are present throughout the depth of 1270D. At higher temperatures strain was localized into gabbro veins cutting peridotite under granulite facies ($>750^\circ\text{C}$) conditions (Figure 7d), during which olivine and pyroxene were crystal plastically deformed. The faults remained active during down-temperature deformation to greenschist-grade conditions ($\sim 300^\circ\text{C}$) during which tremolite and chlorite were deformed by cataclasis and diffusive mass transfer (Figure 7e), and dip between 14° and 54° (ave 38°). This sequence of syn-tectonic alteration minerals and deformation microtextures is nearly identical to that documented on a major detachment fault at 30°N on the Mid-Atlantic Ridge [Schroeder and John, 2004], suggesting that the slope is a major, high-displacement fault surface that denuded peridotite and gabbro (consistent with earlier interpretation). The range of fault dips observed in core may be an indication of rotation by later, secondary faults (such as the brittle faults in 1270A and 1270B), or may reflect a fault with numerous anastomosing splays.

3.3. Site 1271

[13] Holes 1271A and 1271B were drilled west of the axial valley on a >5 km displacement, 10° east-dipping fault scarp (Figure 5). The upper 20 m of

Figure 7. Borehole fault logs (as in Figure 6) with core photos and photomicrographs of selected faults from each hole. Photos: (a) Photomicrograph of cohesive cataclasite from upper fault in Hole 1268A; angular clasts of serpentinite and tremolite/talc schist in a matrix of very fine grained serpentine and fine unidentified minerals. (b) Core photo of peridotite mylonite from ductile fault in at the margin of a gabbro body in Hole 1268A. Fine-grained olivine neoblasts in mylonite have been statically serpentinized, indicating little low-temperature deformation. (c) Photomicrograph of gabbro protomylonite from a zone of diffuse ductile deformation in Hole 1270B. Pyroxene displays bent cleavage, and olivine and pyroxene both exhibit core and mantle texture. (d) Core photo of ductile-to-brittle faults in Hole 1270D. One to three centimeter wide anastomosing shear zones are localized on gabbroic veins cutting relatively undeformed harzburgite. (e) Photomicrograph of ductile-to-brittle shear zones in Hole 1270D. Boudinaged pale-brown hornblende porphyroclasts replace crystal plastically deformed olivine and pyroxene; brown hornblende is cut and replaced by zones of cataclastically deformed tremolite-chlorite schist. (f) Photomicrograph of tremolite-chlorite schist from Hole 1271B. Small porphyroclasts of pale-brown hornblende are present in a matrix of extremely fine grained, schistose tremolite and chlorite that have been deformed dominantly by diffusive mass transfer. (g) Representative core photo of the breccia that defines the upper 56 m of Hole 1272A. Breccia consists of angular clasts of serpentinite, gabbro, basalt, and various ductile and brittle fault rocks that are supported by a matrix of Fe-oxide bearing carbonate. The carbonate displays no deformation microtextures. (h) Core photo of brittle fault in lower half of Hole 1272B. This fault consists of noncohesive serpentinite-dominated gouge, as do most of the ten brittle faults in the lower 75 m of the hole. (i) Core photo of brittle fault from lower portion of Hole 1274A. This fault is typical of the brittle faults logged in Hole 1274, which consist dominantly of noncohesive to semicohesive serpentinite-dominated gouge containing few subangular serpentinite porphyroclasts. (j) Photomicrograph of semiductile-to-brittle fault in upper portion of Hole 1275D. Earliest formed textures show that as strain was localized, green hornblende and plagioclase were deformed simultaneously by crystal plastic flow, diffusive mass transfer, and cataclasis, indicating fault initiation at temperature near the ductile-brittle transition. (k) Semiductile-to-brittle fault in the upper portion of Hole 1275B. Fault was localized into zones of diabase intrusion (diabase on right edge of photomicrograph). Crystal plastically and cataclastically deformed hornblende and plagioclase are intermixed with pods of diabase that appear to have been fragmented while still partially molten.

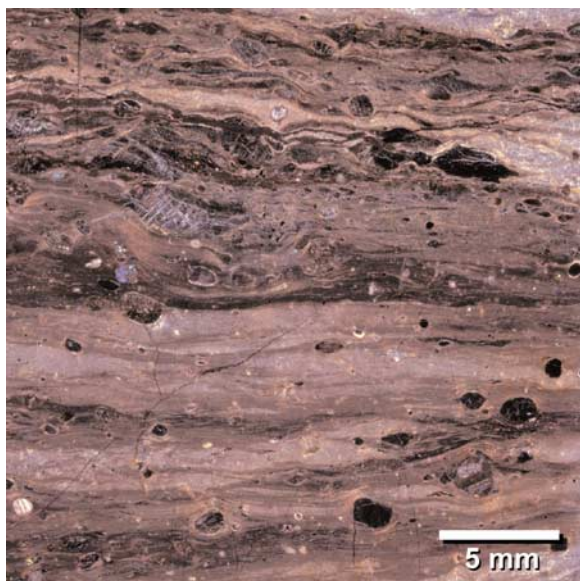


Figure 8. Photomicrograph of a peridotite mylonite sampled on during the MODE98 cruise [Kelemen *et al.*, 1998] on the low-angle slope east of Site 1270. This provides strong support that the slope west of Site 1970 is an exposed fault surface.

Hole 1271B contains abundant semibrittle and brittle fault rocks (tremolite/chlorite schist, serpentine schist and cataclasite; Figures 6 and 7f). Ductily deformed porphyroclasts of pleochroic aluminous amphibole suggest that this fault was initiated as a ductile fault under at least amphibolite grade ($\sim 700^\circ\text{C}$) conditions. Thin ductile shear zones with dips ranging from 11° to 64° are localized on gabbroic dikes and veins throughout the hole. Gabbro dikes wider than 10 cm are not deformed below amphibolite conditions, but many gabbro veins (< 2 cm wide) experienced continuous, down-temperature deformation through the brittle-ductile transition to greenschist grade ($\sim 300^\circ\text{C}$) conditions. The hole also contains a ~ 1 m wide brittle fault consisting of serpentinite gouge at 95 mbsf. The numerous fault types present in this hole suggest a complex tectonic history. Ductile-to-brittle fault rocks most likely represent a major, large-offset fault that was responsible for denuding mantle rocks. Brittle faults may be late-formed splays of the primary long-lived fault, or may be later, second-generation faults that cut the long-lived fault. Another possibility is that some of the faults in the hole were formed by internal block deformation during flexural footwall rotation.

3.4. Site 1272

[14] Site 1272 is located 7 km south of the $15^\circ 20'$ FZ, and ~ 9 km north of Site 1271 (Figure 5). Hole

1272A was drilled west of the axial valley on a 10° east-dipping fault scarp with > 6 km displacement. The upper 56 m of Hole 1272A is a carbonate matrix-supported breccia that contains angular clasts of basalt, diabase, cataclasite, gabbro and serpentinite ranging in diameter from 1 mm to > 1 m. It is unknown if this breccia is sedimentary (landslide-related) or tectonic (fault-related) in origin. If this breccia is a fault zone, it is unlike other faults drilled during Leg 209 in that it does not consist of numerous zones of anastomosing deformation with enclaves of relatively intact rock. Borehole logs from 61–122 mbsf contain ten ~ 1 m wide low resistivity zones, most of which can be correlated to fault rock intervals (gouge, cataclasite, and serpentine schist; Figure 7h) in the core. These faults strike NNW (ave azimuth = 336°), and dip between 22° and 60° to the NE and SW. Though this site recovered no ductile-to-brittle (long-lived) faults, it is located on the same bathymetric structure as Site 1271, which does contain major long-lived faults. It is therefore likely that initial mantle denudation occurred here along a high-displacement normal fault. The brittle faults at this site may be the result of internal block deformation, may be secondary faults that cut a primary fault, and/or may be related to deformation on the nearby $15^\circ 20'$ FZ. The high number of brittle faults present may be partially responsible for the chaotic bathymetry in this area.

3.5. Site 1274

[15] Hole 1274A was drilled west of the axial valley on an 18° east-dipping fault scarp with > 6 km displacement (Figure 4). Several ductile and semibrittle shear zones dipping between 10° and 75° are present in the upper 10 m, but there are no significant intervals of highly deformed rocks at the top of the hole. The hole below 75 mbsf is cut both by minor semibrittle faults and by several major brittle faults. The brittle faults consist of noncohesive serpentinite gouge and/or cohesive cataclasite (Figure 7i). The highest levels of brittle strain are between 75–90 mbsf and 130–145 mbsf. Where present, foliation in the gouge dips at less than 15° . These faults may be splays of a possible, near-surface large fault system that was not recovered in core.

3.6. Site 1275

[16] Site 1275 was drilled on a corrugated, domal massif ~ 28 km to the west of the axial valley at $15^\circ 44' \text{N}$, $46^\circ 54' \text{W}$. The surface of the dome has

been interpreted as a detachment fault with >15 km displacement [MacLeod *et al.*, 2002; Escartín *et al.*, 2003; Fujiwara *et al.*, 2003]. Holes 1275B and D contain mostly gabbro with lesser gabbro-impregnated troctolite. The upper 30 m of each hole contains extensive semibrittle to brittle fault rocks that most likely represent the major detachment fault capping the dome (Figure 4). Strain in this fault appears to have been localized along numerous, thin (0.5–30 cm wide) diabase intrusions at temperatures near the ductile-brittle transition. The presence of rounded diabase fragments in shear zones containing angular plagioclase fragments (Figure 7k) suggests that strain was localized concurrently with liquid diabase intrusion. Similar relationships were observed in this area by Escartín *et al.* [2003]. Shear zones contain both moderate crystal plastic and moderate to extreme cataclastic deformation of hornblende and plagioclase (Figures 7j and 7k), indicating that strain was localized at temperatures very near the brittle ductile transition (typically ~600–700°C for gabbro). Textures indicate continuous down-temperature deformation to greenschist grade (<300°C), as is evidenced by abundant tremolite-talc-chlorite cataclasites and schists. The dip of faults and shear fractures is highly variable (0° to 89°), but the most highly deformed schists and cataclasites generally dip less than 20°. All of the fault rocks in these holes appear to be a part of one single major fault system. There are no textures that indicate multiple periods of activity or cross-cutting by later faults. This contrasts from the other Leg 209 sites, all of which contain evidence for multiple stages of faulting.

4. Discussion

[17] Observations of the drill core recovered during ODP Leg 209 confirm that the upper lithosphere near the 15°20' FZ is primarily composed of peridotite and gabbro and that the seafloor consists of denuded fault surfaces. Holes at six out of the eight sites recovered mostly peridotite and gabbro and contained abundant fault rocks. Holes drilled at sites 1269 and 1273 recovered only basalt. However, these holes penetrated a maximum depth of 26 m, and it is likely that the basalt is only a thin carapace over peridotite or gabbro, as was previously suggested for basalt exposures mapped by submersible [Cannat *et al.*, 1997]. Fault rocks near the surface of some holes can be correlated to surface faults sampled via submersible on earlier

cruises (i.e., peridotite mylonite fault rocks east of Site 1270; Figure 8).

[18] The drill core observations can be used together with the bathymetry to develop a model for lithospheric accretion by faulting with very limited magmatic input. One requirement of any such model is that the style and sequence of faulting must, if retro-deformed, restore the upper lithosphere to a 10–20 km wide zone of upwelling mantle beneath the ridge axis. This necessitates tectonic rotation. Our model incorporates significant rotation of the upwelling mantle for this and several other reasons: (1) it is kinematically the simplest mechanism to make a transition from vertical upwelling to horizontal spreading, (2) post-Curie-temperature rotations of 50° to 80° are documented by anomalous remnant magnetic inclinations at most Leg 209 sites [Garces and Gee, 2007], and (3) analogous highly extended continental rifts show significant degrees of tectonic rotation during normal faulting. The ridges with 1,000–2,000 m relief that dominate the non-volcanic area are spaced by 10–20 km. We suggest that the most likely origin of this bathymetry is denudation of mantle rocks by slip on major faults with a spacing and displacement of similar magnitude to this ridge spacing. The average dip of the major fault surfaces measured in bathymetric cross sections is low (10°–15°). For reasons discussed below, we think that these shallow dipping faults likely rotated from steeper dips in the subsurface [e.g., Buck, 1988; Tucholke *et al.*, 1998; Buck *et al.*, 2005].

[19] We propose that large-displacement faults accommodate much of the extension associated with plate separation at 15°20'N, and argue that the faults are concave downward for a number of reasons:

[20] 1. The effective elastic thickness of the lithosphere even at a cold, slow spreading ridge, is likely to be small (1–2 km) [Escartín *et al.*, 1997, 2001]. Consequently, large displacements on high-angle faults will lead to significant flexural rollover of the faults as the footwall is denuded.

[21] 2. Buck *et al.* [2005] provide a mechanism for amagmatic lithospheric extension in their model for oceanic detachment faulting. On one side of their modeled ridge, all of the extension is accommodated by faulting (their Figure 5b). This model produces large (20 km displacement) faults that show significant roll over. Many faults in Leg 209 core were continuously active from granulite facies

($\sim 900^{\circ}\text{C}$) to subgreenschist facies ($<300^{\circ}\text{C}$) and fault scarps with 10–20 km displacement are visible in bathymetric profiles, consistent with the high-displacement faults in this model.

[22] 3. Up to 80° of sub-Curie-temperature footwall rotation is documented from anomalous magnetic inclinations in cores collected during Leg 209 [Garces and Gee, 2007], consistent with motion on concave-down faults.

[23] 4. Earthquake focal depth solutions from 26° N on the MAR provide further evidence for concave-down faults [deMartin et al., 2005]. At this location, earthquake focal depths dip 70° degrees west beneath the ridge axis and appear to intersect a gently west dipping (15°) plane of earthquake focal depths nearer the surface to the east of the ridge axis. deMartin et al. suggest that the focal depths are consistent with a rolling-hinge fault.

[24] 5. Finally, faults need to be concave-down to accommodate the lithospheric “corner flow” required by plate separation at nonvolcanic ridges (Figure 1b). Concave-down faults permit the restoration of fault slip and the consequent extension at a ridge axis. In order to construct a retro-deformable cross section across the ridge axis, mantle-dominated upper lithosphere must be restorable to the upwelling zone beneath the ridge axis. We made many attempts to construct restorable cross sections using only multiple generations of planar, lower-displacement faults, similar to the model proposed for continental rifts by Proffett [1977]. Retro-deforming these faults produced far greater axial valley relief than is observed, and it was not possible to restore the upper lithosphere to a zone of upwelling mantle. Making faults concave downward requires internal block deformation, but allows the faults to be retro-deformed without generating excess axial relief at the rift valley.

[25] Granulite grade mineral assemblages in many ductile-to-brittle fault rocks suggest that strain localization on the major normal faults begins near the base of the lithosphere. Diffuse, granulite-grade ductile deformation zones in peridotite (i.e., 1270C and D, 1274A) and gabbro (i.e., 1270B) most likely represent widely distributed shear zones. These are localized into highly strained ductile, semibrittle and brittle faults as the footwall is denuded to the surface. In many cases, strain in high-displacement faults was localized on gabbroic or diabase intrusions (i.e., shear zones on gabbroic veins at Sites 1270 and 1271, and faults localized near diabase pods at Site 1275). At any given time,

a major fault is active as both a brittle fault near the surface and as a distributed shear zone at depth as it captures upwelling mantle into its footwall. If major faults were active simultaneously on both sides of the ridge, they may cross-cut and interfere at depth. It is therefore likely that a major fault is active on only one side of the ridge at any given time.

[26] Consequently, our model for nonmagmatic spreading at $15^{\circ}20'$ is asymmetric; at any given time spreading on one side of the ridge will be accommodated by a major, high-displacement, rolling hinge normal fault (manifested in the core as long-lived ductile-to-brittle faults), while spreading on the opposite side of the ridge will be accommodated by many secondary, low-displacement normal faults (manifested in the core as pure brittle faults). The model is a hybrid between rolling-hinge detachment fault models that are based on continental detachment faulting models [e.g., Cann et al., 1997; Blackman et al., 1998; Tucholke et al., 1998], and models for multiple faults with alternating polarity on opposite sides of the ridge axis [e.g., Cannat et al. 1997; Lagabrielle et al., 1998] in that high-displacement faults will flip polarity on timescales of 1 to 5 million years. A suggested faulting sequence is shown in two true-scale, interpretive across-ridge cross sections (Figure 9). In these cross sections, we have interpreted the location of the faults, and have projected them downward using the constraint of bathymetric slope. These cross sections are retro-deformable and consistent with all of our data (petrologic, paleomagnetic and bathymetric).

[27] Spreading on the opposite side of the ridge (in the major fault’s hanging wall) may be accommodated by lithospheric extension over many secondary, lower-offset normal faults. Some of the numerous brittle faults at Sites 1268, 1270, 1271, 1272, and 1274 (Figures 6 and 7) may be such secondary faults. This proposed asymmetric faulting is consistent with asymmetric earthquake distributions documented in this area [Smith et al., 2006]. Smith et al. show that earthquake focal localities extend for a width up to 40 km, starting from one axial valley wall, and extending 10–20 km past the opposite axial valley wall (outside of the axial valley). Most located earthquakes that extend outside the axial valley occur on the side of the ridge that we interpret to be the hanging wall of the currently active major fault (Figure 9). Large-displacement faults most likely evolve from one of the secondary faults when all extensional strain on

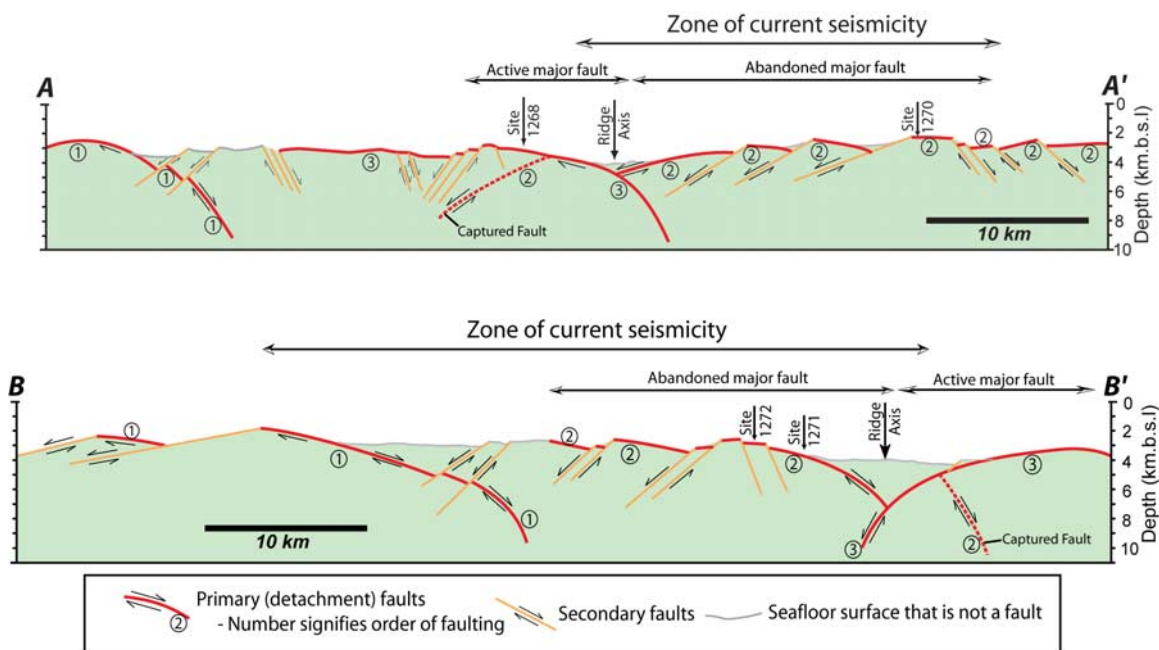


Figure 9. Bathymetric profiles with interpreted fault patterns across the MAR axis. Each profile is a true scale (no vertical exaggeration) representation of the ridge bathymetry. Interpreted primary detachment faults are shown in heavy red lines, secondary faults are shown in yellow lines, and seafloor surfaces that may not represent faults are shown in light gray. Interpreted faults are drawn so that if they are retro-deformed, blocks would form a vertical column of rock in the zone of upwelling mantle beneath the ridge. Numbers on major faults indicate that sequence in which they were active.

its side of the ridge is localized onto that fault. This likely occurs when the lithosphere on the hanging wall side of the ridge reaches a critical point of weakness. This fault may cut the old major fault and end its activity, and spreading on its side of the ridge will then be taken up by secondary faults. This model is similar to the alternating faults model proposed for this area by *Cannat et al.* [1997], but in contrast, it invokes significantly larger fault displacements, requires concave downward faults that enable corner-flow rotation in the footwall, distinguishes between faults with large and small displacement, and requires that active faulting occurs up to 40 km “off axis” on the side of the ridge that is the hanging wall of the active high-displacement fault. If only planar, low- to moderate-displacement faults are used near the ridge axis, as in these earlier models, it is not possible to retro-deform the cross sections to restore the peridotite-dominated upper lithosphere into a column of upwelling mantle beneath the ridge axis. Moreover, invoking only small displacement faults near the ridge axis to denude the mantle is not consistent with the 10–20 km wavelength of the axis-parallel ridges revealed by the bathymetry.

[28] The proposed model is consistent with the complex cross-cutting faults and wide range of fault orientations observed in Leg 209 core (Figures 6 and 7). As illustrated in Figure 9, rock that was originally in the footwall of a large-displacement fault can become part of the footwall or the hanging wall of a secondary fault. Rock in the hanging wall of an earlier large-displacement fault may be incorporated into the footwall of a later large-displacement fault. Major (>10 km displacement) faults most likely correspond to the zones (10 s of meters thick) of ductile to brittle fault rocks recovered from many Leg 209 holes. Other faults present within the core reflect the complexity of deformation predicted by the concave-downward fault model. Flexural footwall rotation of major faults from steep dip at depth to shallow dip near the surface requires both extensional and compressional internal block deformation [Buck, 1988; Buck et al., 2005]. This deformation may account for a minor number shear zones observed in the core that display reverse shear sense indicators. Further, shear zones and faults observed in core that have dips steeper than the dips of faults measured in bathymetry profiles may be a result of internal fault block deformation, thus we prefer to

consider the many small discordant faults in the core as part of the larger fault systems.

[29] Another prediction of our model is asymmetric and somewhat complicated seafloor magnetic anomalies. Rock would be first magnetized during denudation in the footwall of a large-displacement fault. Magnetic anomaly patterns would then be modified and stretched by secondary faulting. The magnetic anomalies recorded for this area [Fujiwara *et al.*, 2003] are asymmetric and very complicated, and thus consistent with our model.

4.1. What About Oceanic Core Complexes?

[30] Corrugated, domal massifs on slow-spreading ridges have been hypothesized to form by detachment faulting, and have been termed “oceanic core complexes” because of their morphologic and geologic similarities to continental metamorphic core complexes [Tucholke and Lin, 1994; Cann *et al.*, 1997; Tucholke *et al.*, 1998; Blackman *et al.*, 1998; MacLeod *et al.*, 2002; Escartín *et al.*, 2003]. Three corrugated domes are present near the 15°20' FZ (Figures 4 and 5). These features were most likely formed by large-displacement faulting, as did the rest of the nonvolcanic area (the smooth, widely spaced ridges).

[31] The relative paucity of oceanic core complexes in the 15°20' area may indicate that particular conditions are required for their formation. If we are correct in suggesting that the widely spaced ridges are generated by large (>10 km) displacement faults, then there must be an additional factor that generates a domal core complex. It is possible that oceanic core complex domes are present where there is locally anomalous magmatism at the ridge axis, i.e., intrusion of relatively large (>10 km diameter) gabbro bodies. Because gabbro is far stronger under greenschist facies conditions than serpentinized peridotite [Escartín *et al.*, 1997, 2001], frozen gabbro plutons may deflect faults around their margins, thus causing doming of the fault surface. Evidence for such deflection of faults around a small gabbro body is present in Hole 1268A, where faults are present in peridotite along both the upper and lower margins of a 20 m wide intrusion.

[32] Drilling results from Leg 209 and other oceanic core complex sites are consistent with this hypothesis. Site 1275 was drilled on a corrugated dome, and contains very different lithologies and fault patterns than the sites that were drilled on the smooth, widely spaced ridges. Site 1275 consists

entirely of gabbro, cumulates, and diabase, while the other sites consist of peridotite with small gabbroic intrusions (Figure 6). Holes at these sites have numerous faults throughout their depth, while Site 1275 holes have highly concentrated deformation near the surface and very little down-hole deformation (Figure 6). The only other corrugated domes drilled to depth on slow spreading ridges (Atlantis Massif on the MAR and Atlantis Bank on the Southwest Indian Ridge) also consist dominantly of gabbro [Dick *et al.*, 1999; Blackman *et al.*, 2006]. Similar relations are also suggested by Ildefonse *et al.* [2006, 2007].

4.2. Ultraslow Spreading Ridges

[33] At ultraslow spreading ridges (<2 mm/yr), conductive cooling from the surface downward leads to the presence of a thick lithosphere and extensive segments exhibiting nonvolcanic bathymetry [Dick *et al.*, 2003]. Consequently, the model presented here may be applicable to these ridges. We predict that the uppermost lithosphere of ultraslow ridges underwent large amounts of tectonic rotation and that similar faulting patterns may be observed. We suggest that the model presented here also may account for the smooth terrain of the easternmost southwest Indian Ridge described by Cannat *et al.* [2006].

5. Conclusions

[34] Seafloor spreading on the Mid-Atlantic Ridge near the 15°20' FZ occurs without sufficient shallow magmatism to generate a coherent magmatic crust. Therefore spreading here is accommodated mostly by extensional faulting. In addition to accommodating horizontal spreading by tectonically denuding mantle peridotite, extensional faults must rotate upwelling mantle by up to 90° (corner flow) in the shallow lithosphere. Wherever mantle peridotite or gabbro is exposed on the seafloor, it can only have been exposed in the footwall of a normal fault. Therefore the seafloor at a gabbro or mantle exposure must be an exposed fault surface. The faulting model presented here can accomplish this while resolving apparent contradictions between the close spacing of faults observed in ODP Leg 209 core, and widely spaced, high-displacement faults suggested by bathymetry patterns.

[35] We argue that the large-scale bathymetry of widely spaced (10–20 km) abyssal hills in the 15°20' area was formed by long-lived normal faults with a similar order of displacement. These major

faults most likely dip steeply beneath the ridge axis into the zone of upwelling mantle, and rotate through a rolling hinge to the gentle dips observed at the surface. Flexural rotation through a rolling hinge requires significant internal block deformation (both compressional and extensional), which formed many of the closely spaced brittle faults observed in core. Because only one major fault is likely to be active at any given time, spreading on the opposite side of the ridge is accommodated by numerous, smaller-displacement, secondary normal faults. These secondary faults may correlate with the steeply dipping brittle faults seen in the core. Slip on a major, high-displacement fault likely continues until the lithosphere on the opposite side of the ridge is thinned and weakened to the point that one of the secondary faults evolves into a new major fault. Thus nonvolcanic spreading in this area is, at any given time, asymmetric, with activity on major, high-displacement faults alternating between one side of the ridge and the other. This model may also apply to other nonvolcanic stretches of slow- and ultra-slow-spreading ridges that exhibit similar bathymetry patterns.

Acknowledgments

[36] We acknowledge the captain and crew of the *JOIDES Resolution*, the Ocean Drilling Scientific Support Staff, and the entire shipboard scientific party of ODP Leg 209. Thank you to Toshiya Fujiwara, who compiled the multibeam sonar data set used in this study. This work was funded by a grant from the Joint Oceanographic Institutions.

References

- Blackman, D. K., J. R. Cann, B. Janssen, and D. K. Smith (1998), Origin of extensional core complexes: Evidence from the Mid-Atlantic Ridge at Atlantis Fracture Zone, *J. Geophys. Res.*, *103*, 21,315–21,333.
- Blackman, D. K., B. Ildefonse, B. E. John, Y. Ohara, D. J. Miller, C. J. MacLeod, and the Expedition 304/305 Scientists (2006), *Proceedings of the Integrated Ocean Drilling Program*, vol. 304/305, Integrated Ocean Drill. Program, College Station, Tex., doi:10.2204/iodp.proc.304305.101.
- Buck, W. R. (1988), Flexural rotation of normal faults, *Tectonics*, *7*, 959–973.
- Buck, W. R., L. L. Lavier, and A. N. B. Poliakov (2005), Modes of faulting at mid-ocean ridges, *Nature*, *434*, 719–723.
- Cann, J. R., D. K. Blackman, D. K. Smith, E. McAllister, B. Janssen, S. Mello, E. Avgerinos, A. R. Pascoe, and J. Escartin (1997), Corrugated slip surfaces formed at North Atlantic ridge-transform intersections, *Nature*, *385*, 329–332.
- Cannat, M. (1993), Emplacement of mantle rocks in the seafloor at mid-ocean ridges, *J. Geophys. Res.*, *98*, 4163–4172.
- Cannat, M., D. Bideau, and H. Bougault (1992), Serpentinized peridotites and gabbros in the Mid-Atlantic Ridge axial valley at 15°37'N and 16°52'N, *Earth Planet. Sci. Lett.*, *109*, 87–106.
- Cannat, M., C. Mével, M. Maia, C. Deplus, C. Durand, P. Gente, P. Agrinier, A. Belarouchi, and G. Dubuisson (1995), Thin crust, ultramafic exposures, and rugged faulting patterns at the Mid-Atlantic Ridge (22°–24°N), *Geology*, *23*, 49–52.
- Cannat, M., Y. Lagabrielle, H. Bougault, J. Casey, N. de Coutures, L. Dmitriev, and Y. Fouquet (1997), Ultramafic and gabbroic exposures at the Mid-Atlantic Ridge: Geological mapping in the 15°N region, *Tectonophysics*, *279*, 193–213.
- Cannat, M., D. Sauter, V. Mendel, E. Ruellan, K. Okino, J. Escartin, V. Combier, and M. Baala (2006), Modes of seafloor generation at a melt-poor ultraslow-spreading ridge, *Geology*, *34*, 605–608.
- Casey, J. F., M. Braun, P. B. Kelemen, T. Fujiwara, T. Matsumoto, and Shipboard Scientific Party (1998), Megamullions along the Mid-Atlantic Ridge between 14° and 16°N: Results of Leg 1, JAMSTEC/WHOI MODE 98 Survey, *Eos Trans. AGU*, *79*(45), Fall Meet. Suppl., F920.
- deMartin, B., R. Reves-Sohn, J. P. Canales, and S. Humphris (2005), Microearthquake survey of the TAG Segment, Mid-Atlantic Ridge (26°N): The early stages of deformation on a detachment fault revealed, *Eos Trans. AGU*, *86*(52), Fall Meet. Suppl., Abstract T33G-03.
- Dick, H. J. B., W. B. Bryan, and G. Thompson (1981), Low-angle detachment faulting and steady-state emplacement of plutonic rocks at ridge-transform intersections (abstract), *Eos Trans. AGU*, *62*, 406.
- Dick, H. J. B., J. H. Natland, and D. J. Miller (1999), *Proceeding of the Ocean Drilling Program, Initial Reports*, vol. 176, Ocean Drill. Program, College Station, Tex.
- Dick, H. J. B., J. Lin, and H. Schouten (2003), An ultraslow-spreading class of ocean ridge, *Nature*, *426*, 405–412, doi:10.1038/nature 02128.
- Escartin, J., and M. Cannat (1999), Ultramafic exposures and the gravity signature of the lithosphere near the Fifteen-Twenty Fracture Zone (Mid-Atlantic Ridge, 14°–16.5°N), *Earth Planet. Sci. Lett.*, *171*, 411–424.
- Escartin, J., G. Hirth, and B. Evans (1997), Effects of serpentinization on the lithospheric strength and the style of normal faulting at slow spreading ridges, *Earth Planet. Sci. Lett.*, *151*, 181–190.
- Escartin, J., G. Hirth, and B. Evans (2001), Strength of slightly serpentinized peridotites: Implications for the tectonics of oceanic lithosphere, *Geology*, *29*, 1023–1026.
- Escartin, J., C. Mével, C. J. MacLeod, and A. M. McCaig (2003), Constraints on deformation conditions and the origin of oceanic detachments: The Mid-Atlantic Ridge core complex at 15°45'N, *Geochem. Geophys. Geosyst.*, *4*(8), 1067, doi:10.1029/2002GC000472.
- Fujiwara, T., J. Lin, T. Matsumoto, P. B. Kelemen, B. E. Tucholke, and J. F. Casey (2003), Crustal evolution of the Mid-Atlantic Ridge near the Fifteen-Twenty Fracture Zone in the last 5 Ma, *Geochem. Geophys. Geosyst.*, *4*(3), 1024, doi:10.1029/2002GC000364.
- Garces, M., and J. Gee (2007), Paleomagnetic evidence of large footwall rotations associated with low-angle faults at the Mid-Atlantic Ridge, *Geology*, *7*, 279–282, doi:10.1130/G23165A.
- Guth, P. L. (2003), Terrain organization calculated from digital elevation models, in *Geomorphology: International Perspectives*, edited by I. S. Evans et al., pp. 199–220, Terrapub, Tokyo.
- Ildefonse, B., D. Blackman, B. E. John, Y. Ohara, D. J. Miller, C. MacLeod, and IODP Expeditions 304/305 Science Party (2006), Oceanic core complexes and crustal accretion at

- slow-spreading ridges: Indications from IODP Expeditions 304–305 and previous ocean drilling results, *Eos Trans. AGU*, 87(52), Fall Meet. Suppl., Abstract B31B–1096.
- Ildefonse, B., D. K. Blackman, B. E. John, Y. Ohara, D. J. Miller, C. J. MacLeod, and the IODP Expeditions 304–305 Scientists (2007), Oceanic core complexes and crustal accretion at slow-spreading ridges, *Geology*, in press.
- Karson, J. A. (1999), Geological investigation of a lineated massif at the Kane Transform Fault: Implications for oceanic core complexes, *Philos. Trans. R. Soc. London, Ser. A*, 357, 713–736.
- Kelemen, P. B., T. Matsumoto, and Shipboard Scientific Party (1998), Geological results of MODE 98, Leg 1: JAMSTEC/WHOI Shinkai 6500 Cruise to 15°N, Mid-Atlantic Ridge, *Eos Trans. AGU*, 79(45), Fall Meet. Suppl., Abstract U22A-18.
- Kelemen, P. B., E. Kikawa, D. J. Miller, et al. (2004), *Proceedings of the Ocean Drilling Program, Initial Reports*, vol. 209, Ocean Drill. Program, College Station, Tex. (Available at http://www-odp.tamu.edu/publications/209_IR/209ir.htm)
- Lagabriele, Y., D. Bideau, M. Cannat, J. A. Karson, and C. Mével (1998), Ultramafic-mafic plutonic rock suites exposed along the Mid-Atlantic Ridge (10°N–30°N): Symmetrical-asymmetrical distribution and implications for seafloor spreading processes, in *Faulting and Magmatism at Mid-Ocean Ridges*, *Geophys. Monogr. Ser.*, vol. 106, edited by W. R. Buck et al., pp. 153–176, AGU, Washington D. C.
- MacLeod, C. J., J. Escartin, D. Banerji, G. J. Banks, M. Gleeson, D. H. B. Irving, R. M. Lilly, A. M. McCaig, Y. Niu, and D. K. Smith (2002), Direct evidence for oceanic detachment faulting at the Mid-Atlantic Ridge, 15°45'N, *Geology*, 30(10), 879–882.
- Matsumoto, T., P. B. Kelemen, and Onboard Scientific Party (1998), Preliminary result of the precise geological and geophysical mapping of the Mid-Atlantic Ridge 14–16°N—Tectonic extension along the magma-poor ridge axis, *Eos Trans. AGU*, 79(45), Fall Meet. Suppl., Abstract U22A-22.
- Proffett, J. M. Jr. (1977), Cenozoic geology of the Yerington District, Nevada, and implications for the nature and origin of Basin and Range faulting, *Geol. Soc. Am. Bull.*, 88, 247–266.
- Ranero, C., and T. J. Reston (1999), Detachment faulting at ocean core complexes, *Geology*, 27, 983–986.
- Rona, F. A., L. Widenfalk, and K. Bostrom (1987), Serpentinized ultramafics and hydrothermal activity along the Mid-Atlantic Ridge crest near 15°N, *J. Geophys. Res.*, 92, 1417–1427.
- Schroeder, T., and B. E. John (2004), Strain localization on an oceanic detachment fault system, Atlantis Massif, 30°N, Mid-Atlantic Ridge, *Geochem. Geophys. Geosyst.*, 5, Q11007, doi:10.1029/2004GC000728.
- Sinton, J. M., and R. S. Detrick (1992), Mid-ocean ridge magma chambers, *J. Geophys. Res.*, 97, 197–216.
- Skolotnev, S. G., N. V. Tsukanov, A. A. Peyve, and Y. A. Raznitismin (1989), 15°20'N fracture zone bedrocks: General characteristics in structure of the Cape Verde Fracture Zone, central Atlantic, *Dokl. Akad. Nauk SSSR*, 439, 40–60.
- Smith, D., and J. R. Cann (1993), Building the crust at the Mid-Atlantic Ridge, *Nature*, 365, 707–715.
- Smith, D., J. R. Cann, and J. Escartin (2006), Widespread active detachment faulting and core complex formation near 13°N on the Mid-Atlantic Ridge, *Nature*, 442, 440–443, doi:10.1038/nature04950.
- Thatcher, W., and D. P. Hill (1995), A simple model for fault generated morphology of slow-spreading mid-oceanic ridges, *J. Geophys. Res.*, 100, 561–570.
- Tucholke, B. E., and J. Lin (1994), A geologic model for the structure of ridge segments in slow-spreading ocean, *J. Geophys. Res.*, 99, 11,937–11,958.
- Tucholke, B. E., J. Lin, and M. C. Kleinrock (1998), Megamullions and mullion structure defining oceanic metamorphic core complexes on the Mid-Atlantic Ridge, *J. Geophys. Res.*, 103, 9857–9866.
- Tucholke, B. E., H. J. Dick, M. A. Tivey, and M. J. Cheadle (2005), Structure of Kane Megamullion, *Eos Trans. AGU*, 86(52), Fall Meet. Suppl., Abstract T33G-01.